

# Precisely computing phonons via irreducible derivatives

Sasaank Bandi and C. A. Marianetti

*Department of Applied Physics and Applied Mathematics, Columbia University, New York, NY 10027*

Computing phonons from first-principles is typically considered a solved problem, yet inadequacies in existing techniques continue to yield deficient results in systems with sensitive phonons. Here we circumvent this issue using the lone irreducible derivative (LID) and bundled irreducible derivative (BID) approaches to computing phonons via finite displacements, where the former optimizes precision via energy derivatives and the latter provides the most efficient algorithm using force derivatives. A condition number optimized (CNO) basis for BID is derived which guarantees the minimum amplification of error. Additionally, a hybrid LID-BID approach is formulated, where select irreducible derivatives computed using LID replace BID results. We illustrate our approach on two prototypical systems with sensitive phonons: the shape memory alloy AuZn and metallic lithium. Comparing our resulting phonons in the aforementioned crystals to calculations in the literature reveals nontrivial inaccuracies. Our approaches can be fully automated, making them well suited for both niche systems of interest and high throughput approaches.

## I. INTRODUCTION

The Born-Oppenheimer potential characterizes the total energy of a collection of nuclei and electrons at zero temperature, where the nuclei are localized at specific positions. The second order Taylor series about some reference configuration provides a vibrational Hamiltonian for the nuclei, from which the phonons may be constructed. Given the importance of phonons for materials properties, precisely and efficiently computing the Taylor series of the Born-Oppenheimer potential from first-principles is critical. While perturbative approaches to computing phonons have their merits, finite displacement approaches are agnostic to the first-principles methodology and their implementations [1]. Therefore, the development of advanced finite displacement methodologies which can knowingly balance precision and efficiency is paramount. Previously, we introduced approaches to computing phonons and their interactions via irreducible derivatives (ID) [1], and here we focus exclusively on phonons and introduce several important technical developments.

Our irreducible approaches begin by building a vibrational Hamiltonian purely in terms of space group irreducible derivatives, such that all space group symmetry and the homogeneity of space (e.g. acoustic sum rules) are satisfied by construction. Each ID will then be associated with the smallest commensurate supercell allowed by group theory, which will require the use of non-diagonal supercells in general. At this stage, the IDs may be constructed via finite difference using either the second energy derivatives or the first force derivatives. The use of energy derivatives implies that each ID is measured independently, and the method which isolates IDs is referred to as the lone irreducible derivative (LID) approach. Alternatively, the use of force derivatives enables multiple IDs to be measured simultaneously, and when the IDs are computed in the fewest number of measurements allowed by group theory, this is referred to as the bundled irreducible derivative (BID) approach. The LID

approach can also be applied to force derivatives, where one computes the smallest number of IDs as possible in a given measurement, and therefore LID with forces can be viewed as a minimal bundling approach. We refer to LID with energy derivatives as  $\text{LID}_0$  and with force derivatives as  $\text{LID}_1$ . Given that energy derivatives normally converge faster than force derivatives with respect to the convergence parameters,  $\text{LID}_0$  is normally more accurate than  $\text{LID}_1$  and BID for a given set of convergence parameters. Moreover,  $\text{LID}_1$  is normally more accurate than BID, given that bundling combines many irreducible representations. Of course, for a given set of convergence parameters, BID is substantially more efficient than  $\text{LID}_1$  which is somewhat more efficient than  $\text{LID}_0$ . Therefore, it is always preferable to use BID, but care is needed to ensure that proper convergence is obtained. In this paper, we derive the best possible way to numerically execute BID, and outline a method to selectively hybridize LID and BID if needed.

When performing a BID calculation, a measurement basis is required to perform finite difference calculations, and there are an infinite number of choices. Previously, we introduced the notion of a condition number optimized (CNO) measurement basis [1], in which there is a minimum amplification of error between the measurements and the irreducible derivatives. However, we did not previously solve the problem of how to find the measurement basis, and in this work we present the solution for second order; demonstrating that zero amplification can be achieved. It should be noted that mainstream finite displacements methods to compute phonons [2–4] are also a type of BID (see [1] for a detailed discussion). However, these approaches are not condition number optimized with respect to the irreducible derivatives, which are the quantities that are most directly probed by experiment (e.g. inelastic neutron scattering).

Given some first-principles theory, different methods for computing phonons may yield different results due to sensitivity, and each method will have a different tradeoff between efficiency and accuracy. In the context of density functional theory (DFT), density functional pertur-

bation theory (DFPT) might be considered the definitive solution, but DFPT still must be converged with respect to various discretization parameters such as  $k$ -points and basis set cutoff, which may be nontrivial. While DFPT has been implemented using the tetrahedron method [5], where convergence was illustrated, widely available implementations of DFPT only incorporate smearing integration methods, which are more difficult to properly extrapolate to zero discretization given that both  $k$ -point density and a smearing parameter must be varied. In any case, results of DFPT must be carefully scrutinized when sensitivities are present. Finite displacement techniques utilize either the energy or the forces, which must be converged with respect to the same discretization parameters, but each observable converges at a different rate. An additional consideration for finite displacement techniques is convergence with respect to the finite displacement discretization  $\Delta$ . If  $\Delta$  is excessively small, impractical values of DFT convergence parameters would be needed, while if  $\Delta$  is excessively large, anharmonic contributions will deviate from leading order. Therefore, it is imperative to execute multiple  $\Delta$  and resolve the known leading order behavior (e.g. quadratic for central finite difference), such that the derivative is precisely extrapolated to  $\Delta = 0$ ; and we refer to this process as the construction of quadratic error tails. The substantial gains in efficiency allowed by our irreducible derivative methods can be converted to gains in precision by properly converging finite displacement calculations in all regards. Moreover, sensitivities are often associated with particular phonon modes (e.g. see Section III), and our approaches inherently isolate such sensitivities; while conventional approaches inherently mix them, making the practical task of converging results much more challenging.

While the LID and BID methods were developed in the context of computing symmetrized displacement derivatives, they can be applied without modification to arbitrary order strain derivatives; which we refer to as  $\epsilon$ -LID and  $\epsilon$ -BID (see Ref. [6] for up to 4th order strain derivatives computed using  $\epsilon$ -LID). Here we only focus on second strain derivatives (i.e. linear elastic constants). Given that the elastic constants dictate the linear phonon dispersion at small  $q$ , precisely computing the elastic constants is an integral component of precisely computing the phonons. When applying  $\epsilon$ -LID and  $\epsilon$ -BID, the strains are symmetrized according to irreducible representations of the point group, such that the usual group theoretical selection rules dictate the strain irreducible derivatives *a priori* (i.e. intrinsic symmetrization [1]). For  $\epsilon$ -LID<sub>0</sub>, the elastic constants are computed using second energy derivatives, while  $\epsilon$ -LID<sub>1</sub> and  $\epsilon$ -BID use first stress derivatives; and  $\epsilon$ -BID measures all irreducible strain derivatives in the fewest measurements possible via bundling. As in the case of phonons,  $\epsilon$ -LID<sub>0</sub> will normally be the most precise approach for a given set of convergence parameters as energy derivatives are easier to converge than stress derivatives, but  $\epsilon$ -BID will be the

most efficient. Conventional approaches for performing high throughput elastic constant calculations are perhaps best considered a type of  $\epsilon$ -LID<sub>1</sub> [7], which is the proper philosophy for high throughput, but  $\epsilon$ -LID<sub>0</sub> should be used when the definitive answer is needed. In this study, all elastic constants are computed using  $\epsilon$ -LID<sub>0</sub>.

To illustrate our methodological developments, we perform calculations on the shape memory alloy AuZn and elemental lithium. We study AuZn in the both the cubic structure (space group 221) and the low symmetry trigonal phase (space group 143) [8], which is formed in a martensitic transition at  $T = 64$  K [9]. The phonons have been extensively explored in the cubic phase using DFT [10], though the results had numerous sensitivities based on the details of the computational approach. We also study lithium in the body centered cubic phase, which behaves as a nearly free electron metal. The phonons have been measured using inelastic neutron scattering [11]. Recent calculations have found several anomalous features in the phonon spectra which are not present in experiment [12], and we will demonstrate that the most substantial anomalies are not present in the numerically precise answer.

## II. BID AND THE CNO MEASUREMENT BASIS

We begin by providing the formulation of BID at second order. Consider a real function  $V(u_1, \dots, u_N)$  invariant to some ambivalent group, where all independent second derivatives must be extracted. Assume that evaluating  $V$  at some arbitrary  $\{u_1, \dots, u_N\}$  has a nontrivial computational cost, but also provides all first derivatives  $\{\frac{\partial V}{\partial u_i}\}$ , also denoted  $\{F_i\}$ , subject to random noise. First order finite difference calculations may then be used to construct second derivatives, which contain random noise from the first derivatives. Define a “measurement vector” as a unit vector in the  $N$  dimensional space of displacements. BID is the method which computes all  $N_d$  independent second derivatives in the smallest number of measurements  $N_m$ . In the absence of symmetry, we have  $N_d = N(N+1)/2$ , but this number will be reduced when the group contains operations other than the identity operation. A measurement along the measurement vector  $\theta_i$  will yield  $N_{v,i}$  nonzero second derivatives, where  $N_{v,i} \leq N$ , which are then stacked into a vector  $\mathbf{v}_i = (\frac{\partial F_1}{\partial \theta_i}, \dots, \frac{\partial F_{N_{v,i}}}{\partial \theta_i})^\top$ . A given  $\mathbf{v}_i$  can then be related to the vector of irreducible derivatives it probes, denoted  $\mathbf{d}_i$ , having dimension  $N_{d,i}$ , via the “chain rule matrix”  $\mathbf{C}_i$  as  $\mathbf{v}_i = \mathbf{C}_i \mathbf{d}_i$ . The number of measurements  $N_m$  is chosen as the smallest number such that  $\sum_{i=1}^{N_m} \text{rank}(\mathbf{C}_i) \geq N_d$ . There will be an infinite number of sets of measurement vectors, and some criteria must be employed to select an optimum choice.

Previously, we introduced the notion of a condition number optimized (CNO) measurement basis [1], whereby the measurement vectors  $\{\theta_1, \dots, \theta_{N_m}\}$  are cho-

sen to minimize the condition number of all  $\mathbf{C}_i$ . The condition number of a matrix can be computed as the ratio of the largest and smallest singular values, and is a measure of the maximum error amplification when solving a linear system of equations. The BID method at second order and the CNO measurement basis is now formally defined, but we are still left with the problem of how to determine the CNO basis.

In order to determine the CNO basis, we consider the group which leaves  $V(u_1, \dots, u_N)$  invariant, and we represent this group in terms of the variables  $\{u_1, \dots, u_N\}$ ; which can then be decomposed into the irreducible representations. At second order, the Great Orthogonality Theorem dictates that there can only be coupling between the same type of irreducible representations, and thus the key quantity will be the maximum number of instances of a given irreducible representation, denoted as  $N_r$ . Given that irreducible representations of the same type must be measured separately, we have  $N_m = N_r$ , and all other irreducible representations can be partitioned into the  $N_m$  bundles. The condition number is naturally minimized by taking equal weights for each irreducible representation in a given bundle, allowing a condition number of one and hence zero amplification of error. For a measurement vector with equal weights, we have  $\theta_i = \mathbf{M}_i \mathbf{x}_i$  where  $\mathbf{M}_i = \frac{1}{\sqrt{N_{\theta,i}}}(1, \dots)$  and  $\mathbf{x}_i$  is the vector of all displaced irreducible representations in the bundle. To construct the chain rule matrix, the partial derivatives  $\frac{\partial x_i}{\partial \theta_i}$  are required, and these are obtained using the pseudoinverse of  $\mathbf{M}_i$ , which is simply  $\mathbf{M}_i^+ = \mathbf{M}_i^T$ . The chain rule matrix is therefore the identity matrix times  $\frac{1}{\sqrt{N_{\theta,i}}}$ , and the condition number is the identity.

We consider several simple examples to illustrate the preceding formulation, beginning with the classical coupled oscillator with mirror symmetry, having potential  $V = \frac{1}{2}(\gamma_A x_A^2 + \gamma_B x_B^2)$ , where  $x_A$  and  $x_B$  are symmetrized modes that transform like irreducible representations of the order 2 group, and  $N_d = 2$ . In this case,  $N_r = 1$  and therefore  $N_m = 1$ . The condition number optimized basis is then obtained by taking equal weights of each irreducible vector, yielding  $\theta_1 = \frac{1}{\sqrt{2}}(x_A + x_B)$ . The irreducible derivatives  $\mathbf{d} = (\gamma_A, \gamma_B)^T$  can be extracted from the measurements  $\mathbf{v} = (\frac{\partial F_A}{\partial \theta_1}, \frac{\partial F_B}{\partial \theta_1})^T$  as  $\mathbf{d} = \frac{1}{\sqrt{2}}\mathbf{v}$ .

The preceding example does not have repeating irreducible representations, so we now consider the three atom oscillator with mirror symmetry, where the potential in terms of the symmetrized modes is  $V = \frac{1}{2}(\gamma_A x_A^2 + \gamma_B x_B^2 + \gamma_{B'} x_{B'}^2 + \gamma_{BB'} x_B x_{B'})$  and  $N_d = 4$ . In this case,  $N_r = 2$  and therefore  $N_m = 2$ . The irreducible derivative  $\gamma_A$  can be bundled into either the measurement of  $\gamma_B, \gamma_{BB'}$  or  $\gamma_{B'}, \gamma_{BB'}$  or both while maintaining a condition number of one. Therefore, a possible condition number optimized basis is  $\theta_1 = \frac{1}{\sqrt{2}}(x_A + x_B)$  and  $\theta_2 = x_{B'}$ . The irreducible derivatives  $\mathbf{d}_1 = (\gamma_A, \gamma_B, \gamma_{BB'})$ , are extracted from the measurement derivatives  $\mathbf{v}_1 = (\frac{\partial F_A}{\partial \theta_1}, \frac{\partial F_B}{\partial \theta_1}, \frac{\partial F_{B'}}{\partial \theta_1})^T$  as  $\mathbf{d}_1 = \frac{1}{\sqrt{2}}\mathbf{v}_1$ . The irreducible deriva-

tives  $\mathbf{d}_2 = (\gamma_{B'}, \gamma_{BB'})$  are extracted from the measurement derivatives  $\mathbf{v}_2 = (\frac{\partial F_{B'}}{\partial \theta_2}, \frac{\partial F_{BB'}}{\partial \theta_2})^T$  as  $\mathbf{d}_2 = \mathbf{v}_2$ . While this example only contains a one dimensional repeating irreducible representation, repeating multidimensional irreducible representations do not require any special attention so long as the same phase convention is employed.

The preceding formalism and examples all pertained to ambivalent groups, which can always have real irreducible representations. The translation group is not ambivalent, and will have complex irreducible representations. However, we will demonstrate that the formulation for ambivalent groups can be applied with trivial modifications. We consider the simplest nontrivial example, which can then be extended via induction. Consider the one dimensional chain with two distinct atoms per unit cell and a system size of 3 unit cells. There will be three  $q$ -points:  $\Gamma$ ,  $\Delta$ , and  $\bar{\Delta}$ . The translationally symmetrized potential energy is given as

$$V = \frac{1}{2} d_{\Gamma\Gamma}^{oo} u_{\Gamma}^o u_{\Gamma}^o + d_{\Delta\Delta}^{aa} u_{\Delta}^a u_{\Delta}^a + d_{\bar{\Delta}\bar{\Delta}}^{bb} u_{\bar{\Delta}}^b u_{\bar{\Delta}}^b + (d_{\Delta\Delta}^{ab} u_{\Delta}^a u_{\bar{\Delta}}^b + c.c.) \quad (1)$$

where  $a, b$  label different instances of the identity representation of the little group at the  $\Delta$  point. While  $d_{\Gamma\Gamma}^{oo}$ ,  $d_{\Delta\Delta}^{aa}$ , and  $d_{\bar{\Delta}\bar{\Delta}}^{bb}$  are real numbers,  $d_{\Delta\Delta}^{ab}$  is complex, and both the real and imaginary parts must be computed. Given that atoms can only be displaced on the real axis, a change of basis is required when performing finite displacement computations. A unitary transformation to the real- $q$  representation is given as

$$u_{q^c} = \frac{1}{\sqrt{2}}(u_q + u_{\bar{q}}), \quad u_{q^s} = \frac{i}{\sqrt{2}}(u_{\bar{q}} - u_q) \quad (2)$$

The potential can be transformed to the real- $q$  representation as

$$V = \frac{1}{2} d_{\Gamma\Gamma}^{oo} u_{\Gamma}^o u_{\Gamma}^o + \frac{1}{2} d_{\Delta\Delta}^{aa} (u_{\Delta^c}^a u_{\Delta^c}^a + u_{\Delta^s}^a u_{\Delta^s}^a) + \frac{1}{2} d_{\bar{\Delta}\bar{\Delta}}^{bb} (u_{\bar{\Delta}^c}^b u_{\bar{\Delta}^c}^b + u_{\bar{\Delta}^s}^b u_{\bar{\Delta}^s}^b) + \Re(d_{\Delta\Delta}^{ab}) (u_{\Delta^c}^a u_{\bar{\Delta}^c}^b + u_{\Delta^s}^a u_{\bar{\Delta}^s}^b) + \Im(d_{\Delta\Delta}^{ab}) (u_{\Delta^c}^a u_{\bar{\Delta}^s}^b + u_{\Delta^s}^a u_{\bar{\Delta}^c}^b). \quad (3)$$

Here we see that the number of measurements is still given by the maximum number of repeating irreducible representations. One choice for the condition number optimized basis is  $\theta_1 = \frac{1}{\sqrt{2}}(u_{\Gamma}^o + u_{\Delta^c}^a)$  and  $\theta_2 = u_{\Delta^c}^b$ . The irreducible derivatives  $\mathbf{d}_1 = (d_{\Gamma\Gamma}^{oo}, d_{\Delta\Delta}^{aa}, \Re(d_{\Delta\Delta}^{ab}), \Im(d_{\Delta\Delta}^{ab}))$ , are extracted from the measurement derivatives  $\mathbf{v}_1 = (\frac{\partial F_{\Gamma}^o}{\partial \theta_1}, \frac{\partial F_{\Delta^c}^a}{\partial \theta_1}, \frac{\partial F_{\Delta^c}^b}{\partial \theta_1}, \frac{\partial F_{\Delta^s}^b}{\partial \theta_1})^T$  as  $\mathbf{d}_1 = \frac{1}{\sqrt{2}}\mathbf{v}_1$ . The irreducible derivative  $\mathbf{d}_2 = (d_{\bar{\Delta}\bar{\Delta}}^{bb})$ , is extracted from the measurement derivatives  $\mathbf{v}_2 = (\frac{\partial F_{\bar{\Delta}^c}^b}{\partial \theta_1})^T$  as  $\mathbf{d}_2 = \mathbf{v}_2$ . In summary, performing a unitary transformation to the real- $q$  basis enables the use of the procedure outlined for ambivalent groups.

In the preceding case, both the real and imaginary parts of the cross derivatives between irreducible representations must be measured. An appropriate gauge transformation can make the cross derivative purely real, but this transformation cannot be known *a priori* in general. However, if the space group has a point symmetry operation that maps  $\mathbf{q} \leftrightarrow \bar{\mathbf{q}}$ , the proper phase convention can be determined *a priori* and then only a real irreducible derivative must be measured. In this case, the number of measurements will be reduced, yielding  $N_m = \lceil N_r/2 \rceil$ . To illustrate this reduction, consider the potential from Eq. 3 but make the atoms equivalent, which results in a mirror plane that maps  $\Delta \leftrightarrow \bar{\Delta}$ . Therefore, a phase convention can be chosen *a priori* such that  $\Im(d_{\Delta\Delta}^{ab}) = 0$ , and  $N_m = 1$ . A condition number optimized basis can be chosen as  $\theta_1 = \frac{1}{\sqrt{3}}(u_\Gamma^o + u_{\Delta c}^a + u_{\Delta s}^b)$ . The irreducible derivatives  $\mathbf{d}_1 = (d_{\Gamma\Gamma}^o, d_{\Delta\Delta}^a, d_{\Delta\Delta}^b, d_{\Delta\Delta}^b)$ , are extracted from the measurement derivatives  $\mathbf{v}_1 = (\frac{\partial F_\Gamma^o}{\partial \theta_1}, \frac{\partial F_{\Delta c}^a}{\partial \theta_1}, \frac{\partial F_{\Delta c}^b}{\partial \theta_1}, \frac{\partial F_{\Delta s}^b}{\partial \theta_1})^\top$  as  $\mathbf{d}_1 = \frac{1}{\sqrt{3}}\mathbf{v}_1$ .

The preceding examples illustrate how to generalize the process of finding the minimal, condition number optimized measurement basis in the one dimensional chain with two atoms per unit cell. However, there are no additional considerations for an arbitrary crystal.

In the preceding we have outlined a condition number optimized measurement basis, and now we present guidelines for resolving a sensitivity associated with a given phonon mode. In our CNO basis, each irreducible derivative can be traced to a specific bundle, and the simplest solution would be to reevaluate the choice of  $\Delta$ 's and or increase the convergence parameters for that particular bundle. However, given that energy derivatives normally converge faster than force derivatives, one could also recompute the problematic irreducible derivatives using LID<sub>0</sub> and use them in place of the erroneous BID result, which we refer to as a hybrid LID-BID approach.

### III. RESULTS

We now illustrate LID, BID, and hybrid LID-BID in several crystals where there are discrepancies compared to the existing literature, including AuZn and body centered cubic Li. Unless otherwise noted, DFT calculations were performed using the Projector Augmented Wave (PAW) method [13, 14], as implemented in the Vienna Ab-initio Simulation Package (VASP) [15–18]. The Perdew, Burke, Ernzerhof generalized gradient approximation (GGA) [19] was used for results in the main text, and local density approximation (LDA)[20] results for AuZn are provided in the Supplemental Material [24]. Unless otherwise noted, a plane wave basis with a kinetic energy cutoff of 1200 eV and 450 eV was employed for Li and AuZn, respectively. A  $\Gamma$ -centered  $k$ -point mesh of  $30 \times 30 \times 30$  for both AuZn and Li. The  $k$ -point in-

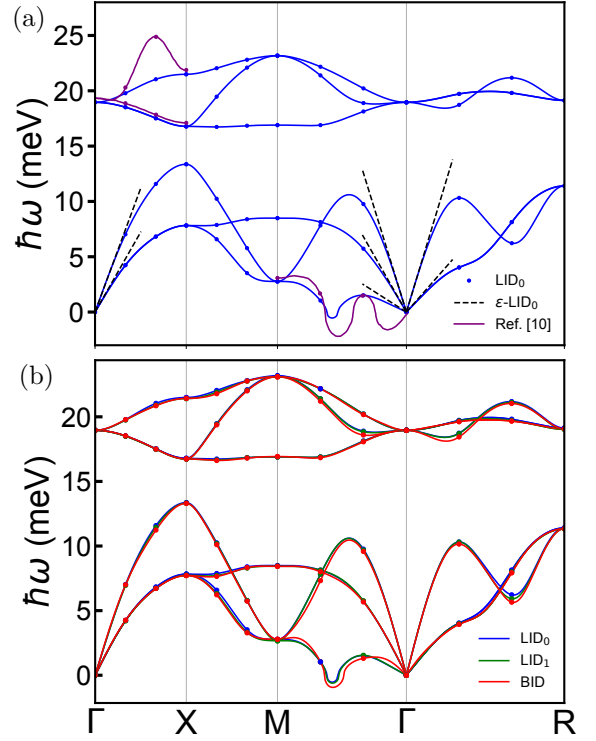


FIG. 1. DFT phonon dispersion of cubic AuZn, where points are computed values and lines are a Fourier interpolation. (a) LID<sub>0</sub> results are shown in blue, black dashed lines are the acoustic dispersion obtained from the elastic constants, and the results shown in purple are taken from Ref. [10]. (b) LID<sub>0</sub>, LID<sub>1</sub>, and BID results are shown in blue, green, and red.

tegrations were done using the tetrahedron method with Blöchl corrections[21]. The DFT energies were converged to within  $10^{-6}$  eV, while ionic relaxations were converged to within  $10^{-5}$  eV. For AuZn, we used the experimental lattice parameter of  $a_0=3.13\text{\AA}$  in order to compare with previous calculations, while energy minimization yielded a lattice parameter of  $2.97\text{\AA}$  for Li and the relaxed trigonal structure of AuZn is provided in Supplemental Material [24]. For the central finite difference calculations within LID and BID, quadratic error tails were constructed using at least eight discretizations (i.e.  $\Delta$  in Eq. 40 in Ref. [1]). It should be noted that many phonon finite difference calculations are performed with forward finite difference and a single discretization, and LID/BID can be executed in this manner, though this choice would not extrapolate the discretization error to zero. Elastic constants were measured using  $\epsilon$ -LID<sub>0</sub>, which uses second strain derivatives of the energy. For LID/BID in Li and cubic AuZn, the Brillouin zone is discretized using a real space supercell of  $8 \times 8 \times 8$  (i.e. multiplicity 512 and 512 atoms) and  $6 \times 6 \times 6$  (i.e. multiplicity 216 and 432 atoms), respectively, which are also denoted  $\hat{\mathbf{S}}_{BZ} = 8\hat{\mathbf{1}}$  and  $\hat{\mathbf{S}}_{BZ} = 6\hat{\mathbf{1}}$ . While LID/BID construct all irreducible derivatives commensurate with  $\hat{\mathbf{S}}_{BZ} = 8\hat{\mathbf{1}}$  and  $\hat{\mathbf{S}}_{BZ} = 6\hat{\mathbf{1}}$



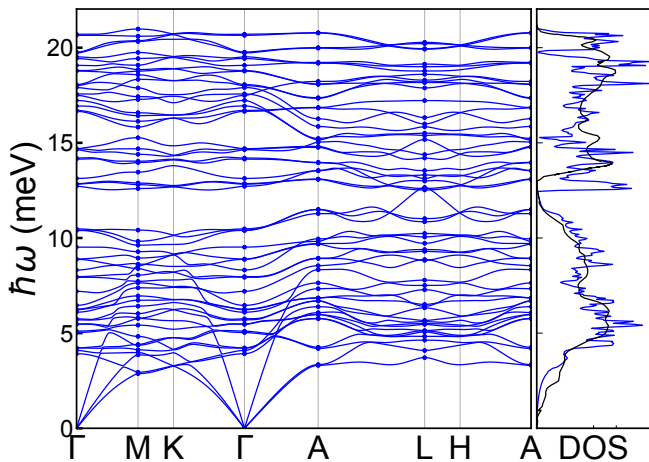


FIG. 2. (a) DFT phonon dispersion of trigonal AuZn computed using BID, where points are computed values and lines are a Fourier interpolation. (b) Phonon DOS from BID (blue) and results from Ref. [23] (black).

in Li and cubic AuZn, respectively, all results are extracted from supercells with multiplicity 8 and 6 [1, 22]. For LID/BID in trigonal AuZn, the Brillouin zone is discretized using  $\hat{\mathbf{S}}_{BZ} = 2\hat{\mathbf{I}}$  (i.e. multiplicity 8 and 144 atoms), and all irreducible derivatives are extracted using supercells with multiplicity 2.

We begin by analyzing the cubic phase of AuZn, where experiment dictates that there is a phase transition to the trigonal structure, which is connected to the cubic structure via a distortion along  $\mathbf{q}$  vectors in the star of  $\mathbf{q} = (\frac{1}{3}, \frac{1}{3}, 0)$ . Inelastic x-ray scattering experiments at  $T = 200$  K indicate that there is a nearly soft phonon mode at  $\mathbf{q} = (\frac{1}{3}, \frac{1}{3}, 0)$  [9], which can be identified as a  $B_2$  mode under the  $C_{2v}$  little group. There are two  $B_2$  basis modes at  $\mathbf{q} = (\frac{1}{3}, \frac{1}{3}, 0)$ , and each can be purely constructed of either Au or Zn, while the eigenmodes will be a linear combination. In order to study the  $B_2$  eigenmodes, one must compute the second derivative of each basis mode and the coupling between the two, resulting in three real irreducible derivatives given that AuZn has inversion symmetry. Therefore, when precisely computing the  $B_2$  eigenmodes, three error tails must be carefully scrutinized.

We proceed by presenting the phonons of the cubic phase of AuZn computed using LID<sub>0</sub> (see Figure 1a). Blue points represent direct measurements of the phonons via LID<sub>0</sub>, solid blue lines are Fourier interpolations, and dashed black lines are the linear dispersion of the acoustic modes obtained independently from the elastic constants computed using  $\epsilon$ -LID<sub>0</sub> (see [24] for error tails). Previously published results [10] using finite displacement are shown as purple lines for branches with major discrepancies. Both sets of results contain all derivatives within the same finite translation group defined by a  $\hat{\mathbf{S}}_{BZ} = 6\hat{\mathbf{I}}$  supercell, and therefore values from Ref. [10] are measured at the same discrete points

as our calculations. Along the plotted directions, the finite displacement measurements from Ref. [10] are in reasonable agreement with our own results, with the major exception of a single spurious point on the highest optical branch between  $\Gamma - X$ ; highlighting the importance of constructing error tails. The resulting Fourier interpolation in Ref. [10] yields imaginary frequencies for the acoustic branches near the  $\Gamma$  point, indicating that the elastic constants are negative. However, our results clearly prove that the elastic constants are positive, and therefore the Fourier interpolation of the finite displacement results from Ref. [10] are likely contaminated by the spurious measurement. The DFPT results from Ref. [10] differ substantially from our results for the lower  $B_2$  branch between  $\Gamma - M$ , and the  $\mathbf{q} = (\frac{1}{3}, \frac{1}{3}, 0)$  point is predicted to be soft. The DFPT and finite displacement results must agree when both are converged. It should be noted that a different pseudopotential was used in the DFPT calculation, which could be the source of some differences. Additionally, the DFPT results used a smearing  $k$ -space integration technique, and it is not clear if the results are converged with respect to the  $k$ -point density. While the GGA results using the VASP PAWs and the experimental lattice parameter do not yield a soft mode, using LDA under these conditions will yield a soft mode [24]. Additionally, using GGA with the relaxed lattice parameter will also yield a soft mode. Therefore, the physics of the  $B_2$  mode is somewhat sensitive and requires a detailed investigation to provide a robust comparison with experiment.

Having established the precise phonon spectrum using LID<sub>0</sub>, we now proceed to assess the precision of BID using the CNO basis and LID<sub>1</sub> (see Figure 1b). Given the importance of the  $B_2$  modes at  $\mathbf{q} = (\frac{1}{3}, \frac{1}{3}, 0)$ , we will retain the LID<sub>0</sub> result for the two dimensional  $B_2$  block, and all other results will be obtained from BID and LID<sub>1</sub>, respectively. We see that LID<sub>1</sub> and BID only introduce small errors, though the magnitude of the errors are always larger in BID, as expected.

We now proceed to the trigonal phase of AuZn, where the phonons are computed using BID with  $C_1$  symmetry (see Figure 2). The only previous result in the literature that we are aware of is a phonon DOS [23], which we directly compare with. There is a notable difference in that the results from Ref. [23] are missing a substantial peak in the DOS at approximately 12.75 meV. A relevant difference between our calculations is the fact that Ref. [23] computes all irreducible derivatives associated with a  $2 \times 2 \times 1$  supercell while we compute all irreducible derivatives associated with a  $2 \times 2 \times 2$  supercell. However, we have confirmed that there is still a peak using only the irreducible derivatives from  $2 \times 2 \times 1$  [24]. Another major difference is that we construct quadratic error tails while Ref. [23] uses a single  $\Delta$ , which can cause discretization errors. A final difference is that our relaxed structure has some nontrivial differences from Ref. [23], despite the fact that our DFT cutoff parameters are similar, and this could account for some differences.

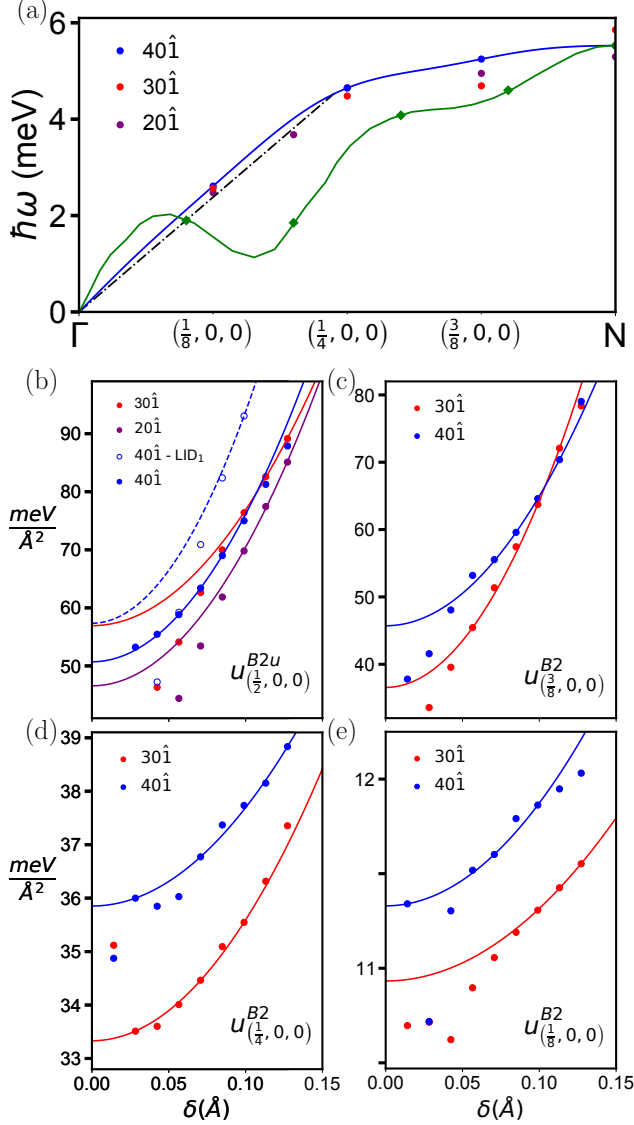


FIG. 3. (a) DFT phonons of Li for the lowest branch along  $\Gamma$ -N computed using BID, where points are computed values and lines are a Fourier interpolation. BID results are provided for  $k$ -point meshes of  $20\hat{1}$ ,  $30\hat{1}$ , and  $40\hat{1}$ , and results from Ref. [12] are shown in green. Panels (b), (c), (d), and (e) show plots of energy vs. displacement magnitude for symmetrized mode amplitudes  $u_{(\frac{1}{2}, 0, 0)}^{A2g}$ ,  $u_{(\frac{3}{8}, 0, 0)}^{B1u}$ ,  $u_{(\frac{1}{4}, 0, 0)}^{B1u}$ , and  $u_{(\frac{1}{8}, 0, 0)}^{B1u}$ , where  $\delta$  is the real space amplitude which is modulated throughout the supercell as  $\delta \cos(2\pi \mathbf{q} \cdot \mathbf{t})$ . Various  $k$ -point meshes are computed, and force derivatives are included in panel b. The intercepts yield the irreducible derivative of the respective mode.

We now consider the phonons of Li metal in the body-centered cubic phase, and we begin by focussing on the lowest frequency branch between  $\Gamma$  and N (see Figure 3a), as unusual results were obtained in previously published work [12]. We follow our established protocol of investigating with LID<sub>0</sub>, and the task is to ensure proper

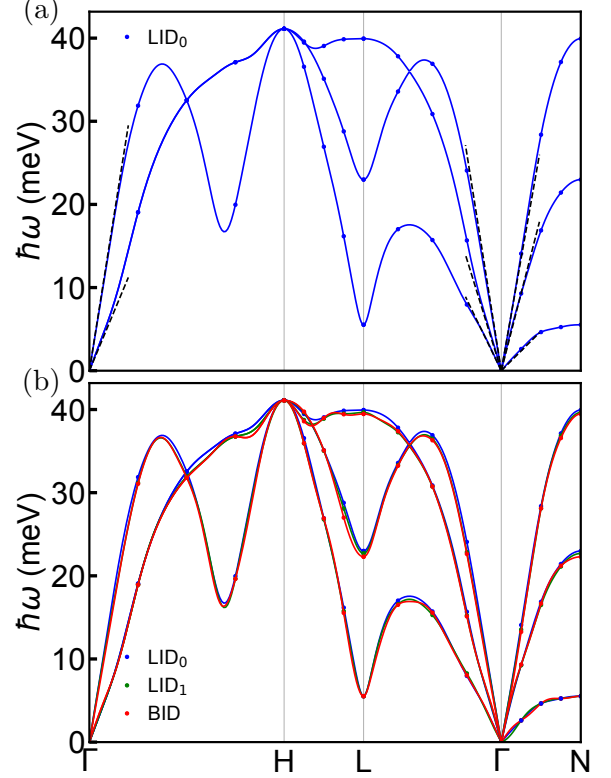


FIG. 4. DFT phonon dispersion of body centered cubic Li, where points are computed values and lines are a Fourier interpolation. (a) LID<sub>0</sub> results are shown in blue and the acoustic dispersion obtained from the elastic constants are black lines. (b) LID<sub>0</sub>, LID<sub>1</sub>, and BID results are shown in blue, green, and red.

error tails are obtained, which mainly involves including a sufficient density of  $k$ -points. In Fig. 3a, circular points represent direct measurements of the phonons via LID<sub>0</sub> at various  $k$ -point mesh densities, the blue line is a Fourier interpolation of  $\hat{\mathbf{S}}_{BZ} = 8\hat{1}$  using an electronic  $k$ -point mesh of  $40\hat{1}$ , and the dashed black line is the linear dispersion of the acoustic mode obtained from the  $\epsilon$ -LID<sub>0</sub> elastic constants. The results of Ref. [12] using finite displacement calculations with  $\hat{\mathbf{S}}_{BZ} = 10\hat{1}$  are shown as green diamonds and lines for the measured and interpolated results, respectively. Most notably, the modulations in the Ref. [12] results are not observed in our highest precision  $40\hat{1}$   $k$ -point mesh results. Given that  $\hat{\mathbf{S}}_{BZ} = 8\hat{1}$  and  $\hat{\mathbf{S}}_{BZ} = 10\hat{1}$  are not commensurate for the interior points, we also measure  $\mathbf{q} = (\frac{1}{5}, 0, 0)$  using a  $20\hat{1}$   $k$ -point mesh, which yields a result which still appears to be in the linear dispersion regime; ruling out an anomaly at this particular  $\mathbf{q}$  point. The most obvious difference between our LID<sub>0</sub> calculations and those of Ref. [12] is that the former uses second energy derivatives and quadratic error tails while the latter uses first

force derivatives and a single  $\Delta$ . Both of these differences are likely to contribute to the modulations in Ref. [12]. However, even our results show a fair amount of variation on going from  $20\hat{1}$  to  $30\hat{1}$  to  $40\hat{1}$   $k$ -point mesh densities for  $\mathbf{q} = (\frac{3}{8}, 0, 0)$  and  $\mathbf{q} = (\frac{1}{2}, 0, 0)$ . Therefore, it is interesting to explore the error tails (Fig. 3, panels *b-e*). For the case of  $\mathbf{q} = (\frac{1}{2}, 0, 0)$  (panel *b*), the  $k$ -mesh of  $20\hat{1}$  strongly deviates from a quadratic below  $\delta = 0.1$  Å, indicating that fitting larger  $\delta$  to a quadratic error tail is critical to obtaining reasonable results at this  $k$ -point density; and a similar assessment holds for  $30\hat{1}$ . However, increasing to  $40\hat{1}$  yields a clear quadratic behavior down to  $\delta = 0.02$  Å. It is also instructive to evaluate the corresponding LID<sub>1</sub> force derivative for  $40\hat{1}$ , which does not show signs of quadratic behavior until large  $\delta$ , demonstrating the limitation of force derivatives. Given the notable variations at  $\mathbf{q} = (\frac{3}{8}, 0, 0)$ , it is also useful to explore the corresponding error tails (see panel *c*), where  $30\hat{1}$  only has an average quadratic fit while  $40\hat{1}$  has four consecutive points which are strongly quadratic. The quadratic behavior for  $30\hat{1}$  and  $40\hat{1}$  in  $\mathbf{q} = (\frac{1}{8}, 0, 0)$  and  $\mathbf{q} = (\frac{1}{4}, 0, 0)$  is comparable and the overall changes of the intercept are small (see panels *d* and *e*). Overall, we have demonstrated that there is a notable sensitivity to the  $k$ -point mesh density for  $\mathbf{q} = (\frac{3}{8}, 0, 0)$  and  $\mathbf{q} = (\frac{1}{2}, 0, 0)$ . However,  $\mathbf{q} = (\frac{1}{8}, 0, 0)$  and  $\mathbf{q} = (\frac{1}{4}, 0, 0)$  do not appear sensitive, and the former is in reasonable agreement with the linear dispersion given by the elastic constants. It is also worth noting that early calculations of phonons from DFT did not show these modulations [25], nor are these features observed at  $T = 98$  in inelastic neutron scattering measurements [11].

We now proceed to compute the entire phonon spectrum using LID<sub>0</sub> (see Figure 4*a*). Given the sensitivity observed in Fig. 3, we retain the highest precision  $40\hat{1}$   $k$ -point mesh results for the irreducible derivatives in this branch, and we use  $30\hat{1}$  otherwise. We see that the results are in good agreement with the linear acoustic dispersions from the elastic constants at small  $\mathbf{q}$ . Having established the LID<sub>0</sub> results, we now proceed to assess the precision of LID<sub>1</sub> and BID using the CNO basis (see Figure 4*b*). Once again, we retain highest precision  $40\hat{1}$  LID<sub>0</sub> results for the irreducible derivatives in the branch studied in Fig. 3. We begin by exploring LID<sub>1</sub> to isolated the effect of using first derivatives of the forces in place of second derivatives of the energy. We see that LID<sub>1</sub> only introduces small changes, such as near the  $M$ -point. These differences are small enough for our purposes, but

they could be reduced further by increasing the various convergence parameters of the calculation. In the BID result, where the effect of bundling can be seen by comparing the red curve with the green curve, one can see that the magnitude of the changes are on the same scale as the effect of using forces. Here we see that the large reduction in computational cost is achieved without any appreciable loss in fidelity.

#### IV. CONCLUSION

In summary, we have demonstrated how to accurately and efficiently compute phonons using the LID and BID approaches. In previous work, we defined the notion of a condition number optimized bundled basis, but did not provide a method to find an optimal solution [1]. Here we derived an optimal solution at second order, enabling BID to provide irreducible derivatives in the smallest number of computations with zero amplification of error. Typically, one will use BID to compute all irreducible derivatives. If there are known sensitivities, or if BID error tails are deficient, LID<sub>0</sub> (i.e. using energy derivatives) can be used to compute the problematic irreducible derivatives, replacing the BID result. This hybrid LID-BID approach balances accuracy and efficiency as needed.

We demonstrated the fidelity of our irreducible approaches by addressing sensitive phonons from the literature. In elemental Li, we computed the phonons and confirm a sensitivity in the lowest phonon branch between  $\Gamma$  and  $N$ , which can be properly resolved using LID<sub>0</sub> with a very fine electronic  $k$ -point mesh along with quadratic error tails. In the cubic phase of AuZn, we compute the phonons and demonstrate consistency with the elastic constants computed using LID<sub>0</sub>, and resolve the discrepancies in previous calculations. We also compute the phonons in the trigonal phase of AuZn. Our irreducible methods allow one to convert gains in efficiency into gains in accuracy, providing the definitive solution for the computed phonons in Li and AuZn.

#### V. ACKNOWLEDGEMENTS

This work was supported by the grant DE-SC0016507 funded by the U.S. Department of Energy, Office of Science. This research used resources of the National Energy Research Scientific Computing Center, a DOE Office of Science User Facility supported by the Office of Science of the U.S. Department of Energy under Contract No. DE-AC02-05CH11231.

- 
- [1] L. Fu, M. Kornbluth, Z. Cheng, and C. A. Marianetti, Group theoretical approach to computing phonons and their interactions, *Phys. Rev. B* **100**, 014303 (2019).
  - [2] K. Parlinski, Z. Li, and Y. Kawazoe, First-principles determination of the soft mode in cubic zro2, *Phys. Rev.*

*Lett.* **78**, 4063 (1997).

- [3] D. Alfe, Phon: a program to calculate phonons using the small displacement method, *Computer Physics Communications* **180**, 2622 (2009).

- [4] A. Togo and I. Tanaka, First principles phonon calculations in materials science, *Scripta Materialia* **108**, 1 (2015).
- [5] M. Kawamura, Y. Gohda, and S. Tsuneyuki, Improved tetrahedron method for the brillouin-zone integration applicable to response functions, *Phys. Rev. B* **89**, 094515 (2014).
- [6] M. A. Mathis, A. Khanolkar, L. Fu, M. S. Bryan, C. A. Dennett, K. Rickert, J. M. Mann, B. Winn, D. L. Abernathy, M. E. Manley, D. H. Hurley, and C. A. Marianetti, Generalized quasiharmonic approximation via space group irreducible derivatives, *Phys. Rev. B* **106**, 014314 (2022).
- [7] M. D. jong, W. Chen, T. Angsten, A. Jain, R. Notestine, A. Gamst, M. Sluiter, C. K. Ande, S. Van\_der\_zwaag, J. J. Plata, C. Toher, S. Curtarolo, G. Ceder, K. A. Persson, and M. Asta, Charting the complete elastic properties of inorganic crystalline compounds, *Scientific Data* **2**, 150009 (2015).
- [8] T. Makita, A. Nagasawa, Y. Morii, N. Minakawa, and H. Ohno, Phonon-dispersion relations of premartensitic beta(1)-phase in auzn alloys, *Physica B-condensed Matter* **213**, 430 (1995).
- [9] J. C. Lashley, S. M. Shapiro, B. L. Winn, C. P. Opeil, M. E. Manley, A. Alatas, W. Ratcliff, T. Park, R. A. Fisher, B. Mihaila, P. Riseborough, E. K. H. Salje, and J. L. Smith, Observation of a continuous phase transition in a shape-memory alloy, *Phys. Rev. Lett.* **101**, 135703 (2008).
- [10] L. Isaeva, P. Souvatzis, O. Eriksson, and J. C. Lashley, Lattice dynamics of cubic auzn from first principles, *Phys. Rev. B* **89**, 104101 (2014).
- [11] H. Smith, G. Dolling, R. Nicklow, P. Vijayaraghavan, and M. Wilkinson, *Proc. conf. on inelastic neutron scattering*, p. 149.
- [12] M. Hutcheon and R. Needs, Structural and vibrational properties of lithium under ambient conditions within density functional theory, *Phys. Rev. B* **99**, 014111 (2019).
- [13] P. E. Blochl, Projector augmented-wave method, *Phys. Rev. B* **50**, 17953 (1994).
- [14] G. Kresse and D. Joubert, From ultrasoft pseudopotentials to the projector augmented-wave method, *Phys. Rev. B* **59**, 1758 (1999).
- [15] G. Kresse and J. Hafner, Abinitio molecular-dynamics for liquid-metals, *Phys. Rev. B* **47**, 558 (1993).
- [16] G. Kresse and J. Hafner, Ab-initio molecular-dynamics simulation of the liquid-metal amorphous-semiconductor transition in germanium, *Phys. Rev. B* **49**, 14251 (1994).
- [17] G. Kresse and J. Furthmuller, Efficiency of ab-initio total energy calculations for metals and semiconductors using a plane-wave basis set, *Computational Materials Science* **6**, 15 (1996).
- [18] G. Kresse and J. Furthmuller, Efficient iterative schemes for ab initio total-energy calculations using a plane-wave basis set, *Phys. Rev. B* **54**, 11169 (1996).
- [19] J. P. Perdew, K. Burke, and M. Ernzerhof, Generalized gradient approximation made simple, *Phys. Rev. Lett.* **77**, 3865 (1996).
- [20] J. P. Perdew and A. Zunger, Self-interaction correction to density-functional approximations for many-electron systems, *Phys. Rev. B* **23**, 5048 (1981).
- [21] P. E. Blochl, O. Jepsen, and O. K. Andersen, Improved tetrahedron method for brillouin-zone integrations, *Phys. Rev. B* **49**, 16223 (1994).
- [22] J. H. Lloyd-williams and B. Monserrat, Lattice dynamics and electron-phonon coupling calculations using nondiagonal supercells, *Phys. Rev. B* **92**, 184301 (2015).
- [23] M. Sanati, R. C. Albers, T. Lookman, and A. Saxena, First-order versus second-order phase transformation in auzn, *Physical Review B* **88**, 024110 (2013).
- [24] See Supplemental Material at [URL will be inserted by publisher] for error tails, plane wave cutoff and  $k$ -point convergence, select LDA results, and irreducible derivatives.
- [25] J. P. Perdew and S. H. Vosko, Phonon frequencies of lithium from a local effective potential, *Journal Of Physics F-metal Physics* **6**, 1421 (1976).